Multiple cis-regulatory elements collaborate to control *mdka* expression in telencephalic neural stem of adult zebrafish during constitutive and regenerative neurogenesis

Jincan Chen[1], Masanari Takamiya[1], Agnes Hendriks[1], Tanja Beil[1], Csilla Varnai[2] Nicolas Diotel[3] and Sepand Rastegar[1,*]

1 Institute of Biological and Chemical Systems-Biological Information Processing (IBCS-BIP), Karlsruhe Institute of Technology (KIT), Karlsruhe, Germany
2 Department of Cancer and Genomics Sciences, University of Birmingham, Birmingham, United Kingdom
3 Université de La Réunion, INSERM, UMR 1188, Diabète athérothrombose Thérapies Réunion Océan Indien (DéTROI), Saint-Pierre, La Réunion, France

*Correspondence to:
S. Rastegar, Institute of Biological and Chemical Systems-Biological Information Processing (IBCS-BIP), Karlsruhe Institute of Technology, Karlsruhe 76344, Germany. Tel: +49 721 608 22507. E-mail: sepand.rastegar@kit.edu.

Running title: Transcriptional regulation of *mdka* in the nervous system

Keywords: Neurogenesis; Radial glial cells; Regeneration; Zebrafish; *mdka*; Cis-regulatory elements; Gene transcription regulation

Abbreviations: CRE: cis-regulatory element; dpf: days post-fertilization; Dm: dorsomedial of the telencephalon; dpl: days post-lesion; EGFP: enhanced green fluorescent protein; FISH: fluorescent *in situ* hybridization; hpf: hours post-fertilization; IHC: immunohistochemistry; kb: kilo bases; PCNA: proliferating cell nuclear antigen; RGCs: radial glial cells; mRNA: messenger RNA; *mdka*: *midkine a*; NSCs: neural stem cells; S100β: S100 calcium-binding protein β; *Tg*: transgenic line; TSS: transcription start site; VZ: ventricular zone;

Abstract

Zebrafish is a powerful animal model for studying nervous system regeneration due to its remarkable regenerative abilities and the availability of diverse molecular tools. After telencephalic brain injury, neural stem cells (NSCs) in the ventricular zone (VZ) become activated, proliferate, and generate new neurons essential for brain repair. However, the molecular mechanisms regulating these processes remain unclear. Here, we investigate the transcriptional regulation of *midkine-a* (*mdka*), a heparin-binding growth factor gene encoding the secreted protein Midkine-a (Mdka), which is upregulated after injury in radial glial cells (RGCs), the bona fide NSCs of the adult zebrafish telencephalon. Using genome-wide bioinformatic analysis, we identified six putative cis-regulatory elements (CREs) associated with *mdka*. Transgenic assays revealed that these CREs coordinate *mdka* expression during both development and regeneration. In the zebrafish embryo, CRE2, CRE3, CRE4, and CRE6 are required for EGFP expression in the nervous system, with CRE3 showing the strongest activity. In the adult telencephalon, CRE2, CRE4, and CRE6 are active in NSCs, with CRE2 best mimicking *mdka* expression at the ventricular zone. Importantly, individual CREs could not fully reproduce endogenous *mdka* expression, especially under regenerative conditions. In contrast, a combined CRE2346 construct closely recapitulated *mdka* expression in both the embryo and adult telencephalon under homeostatic conditions. These results suggest that *mdka* expression is controlled by a modular and cooperative cis-regulatory architecture that enables precise gene regulation during development, telencephalon homeostasis, and regeneration.

52 **Introduction**

53 Understanding the molecular mechanisms underlying tissue and organ regeneration
54 is critical for addressing the growing challenges posed by neurodegenerative
55 diseases, such as dementia, Parkinson's, and Alzheimer's. These diseases place a
56 significant medical and societal burden on an aging population, underscoring the
57 urgent need for effective therapeutic strategies to address these conditions. Zebrafish
58 has emerged as a key vertebrate model for studying regeneration due to its
59 exceptional ability to regenerate tissues throughout both embryonic and adult stages
60 [1-6]. Unlike most mammals, zebrafish can regenerate organs like the heart, fin, retina,
61 spinal cord, and specific brain regions without scarring and obvious disabilities, which
62 makes them invaluable for studying regenerative processes [2]. With over 70% genetic
63 similarity to humans [7] and a vast number of mutants [8], transgenic lines [9-11], and
64 genomic resources such as the DANIO-CODE Data Co-Ordination Center (DCC)
65 (https://danio-code.zfin.org/), zebrafish provide a unique platform to study gene
66 function, regulation, and cellular dynamics during embryonic development, adulthood
67 under homeostatic and regenerative conditions [12-14]. In zebrafish, the adult
68 telencephalon regenerates by activating dormant RGCs in the ventricular zone (VZ),
69 which produce new neurons to replace those lost from injury [15, 16]. Recent
70 transcriptomic studies have identified several genes significantly upregulated following
71 injury [17-20], one of the most notable being *midkine-a* (*mdka*), a heparin-binding
72 growth factor with multiple roles in development, repair and diseases [21-23].
73 Interestingly, *mdka* expression increases in quiescent RGCs after telencephalic injury,
74 resembling the behaviour of *id1* (*inhibitor of differentiation 1*) [21], a transcriptional
75 regulator downstream of the BMP signalling pathway [24, 25]. Both *mdka* and *id1* are
76 predominantly expressed in quiescent type 1 cells (RGCs) and are absent in type 2
77 cells corresponding to actively dividing cells [21]. Both type 1 and type 2 cells express
78 glial markers such as S100β and GFAP, while type 2 cells in addition express the
79 proliferation marker PCNA (proliferating cell nuclear antigen). Lineage tracing
80 experiments have demonstrated that type 2 cells differentiate into type 3 neuroblasts,
81 which migrate and mature into specific neuronal types [26, 27].

82 Beyond the brain, *mdka* has been implicated in the regeneration of other tissues in
83 zebrafish and other vertebrates, including the heart, fin, and retina, suggesting that it

may play a common role in the regenerative process [28-35]. The zebrafish *midkine* family includes two genes: *mdka* and its paralog *midkine b* (*mdkb*), the result of a gene duplication event [36]. However, only *mdka* is significantly upregulated after injury, highlighting its specific role in regenerative responses [21]. This study investigates the transcriptional regulation of *mdka* in the zebrafish telencephalon, focusing on its regulation in NSCs during neurogenesis and regeneration. We aim to uncover the molecular mechanisms behind its transcription by identifying and characterizing cis-regulatory elements (CREs) that control *mdka* expression in both homeostatic and regenerative contexts.

Our findings, using genome-wide bioinformatic approaches and validation by transgenesis, reveal that multiple CREs work together to regulate *mdka* expression. In embryos, CRE2, CRE3, CRE4, and CRE6 are critical for nervous system expression, while in the adult telencephalon, CRE2, CRE4, and CRE6 are essential for expression in NSCs. Notably, none of the CREs alone were sufficient to fully recapitulate *mdka* expression in the embryonic nervous system or adult telencephalon. These findings highlight the complexity of *mdka* regulation, where individual CREs contribute differently to expression patterns depending on molecular and environmental signals. Furthermore, a transgenic EGFP reporter line containing CRE2, CRE3, CRE4, and CRE6 best mimicked endogenous *mdka* expression in both zebrafish embryos and the adult telencephalon under homeostatic and regenerative conditions, emphasizing the role of multiple molecular cues in *mdka* regulation.

Results

Identification and characterization of *mdka* CREs in the zebrafish embryo

To investigate the transcriptional regulation of *mdka*, we conducted a systematic search for CREs controlling *mdka* expression in zebrafish embryos at 24 hours post-fertilization (hpf) and in the ventricular zone of the adult telencephalon under both physiological and injury-induced conditions. Using data from the DANIO-CODE repository [14, 37], we identified six potential CREs located upstream, downstream, or in intergenic regions of the *mdka* coding sequence, as shown in **Figure 1**. These regions were selected based on chromatin accessibility, as assessed by ATAC-seq (Assay for Transposase-Accessible Chromatin with sequencing) across zebrafish developmental stages, from dome to long-pec. We also considered sequence conservation with the carp genome [38], indicated by blue boxes. Based on epigenetic features provided in the DANIO-CODE resource, including DNA methylation and histone modifications, the potential CREs were classified as promoters or enhancers and categorized by their activation state (repressed, quiescent, or activated) and strength (weak or strong). To validate their regulatory activity *in vivo*, each CRE was cloned upstream of a 1.0-kb *gata2* minimal promoter, corresponding to the most truncated basal promoter (P5) described by Meng et al. (1997) [39]. This promoter has been subsequently validated for enhancer assays by Navratilova et al. (2009) and Zhang et al. (2020) [25, 40], and was used here to drive EGFP expression (**Figure 2A**). These constructs were introduced into zebrafish germline cell to generate stable transgenic lines, *Tg(CREx-gata2aPR:EGFP)*, where CREx represents one of the identified CREs (**Figure 2A**). Five of the six CREs (CRE2-6) drove expression in 24 hpf zebrafish embryos, displaying partially overlapping patterns with endogenous *mdka* expression (**Figure 2B-G; B'-G'; Figure S1A, B**). Among them, *Tg(CRE3-gata2aPR:EGFP)* most closely recapitulated *mdka* expression (**Figure 2D, D'** and **Table 1**). In this line, EGFP was detected along the spinal cord, tail/fin fold, and brain (**Figure 2D, D'; Table 1; Figure S1A** shows a representative 24 hpf zebrafish embryo with specific anatomical regions). However, none of the individual CREs fully replicated the endogenous *mdka* expression pattern (**Figure 2; Table 1**). No EGFP expression was detected in the stable lines generated with CRE1 **(Figure 2B, B')**. Several explanations could account for this, including the possibility that CRE1

137 functions as a silencer. This hypothesis will be briefly discussed in the relevant section.
138 Additionally, each CRE was tested in combination with three different promoters: the
139 *ctgf* promoter [41], the zebrafish synthetic promoter (zsp) [42], and the *mdka* intrinsic
140 promoter (mdkaPR, this study). EGFP expression in these transient transgenics
141 closely resembled that observed using the *gata2a* promoter (**Figure S2**), supporting
142 the conclusion that EGFP expression is primarily driven by the CREs rather than by
143 the specific promoter used. Given the consistent expression patterns observed with
144 the *gata2a* promoter, all subsequent characterization of the CREs was carried out
145 using the *gata2aPR:EGFP* construct.

146 **Characterization of CREs driving *mdka* expression in adult NSCs**

147 In the adult zebrafish telencephalon, EGFP expression was detected in four out of six
148 transgenic lines generated (**Figure 3C, C'; D, D'; E, E'; G, G'**). No expression was
149 observed for CRE1 and CRE5 (**Figure 3B, B'; F, F'**). CRE3 drove strong ectopic
150 EGFP expression in the dorsal pallium (Dp) and lateral pallium (Dl), whereas no
151 expression was detected in the dorsomedial region (Dm) of the VZ (**Figure 3D, D'**). In
152 contrast, CRE2, CRE4, and CRE6 directed EGFP expression in the VZ of the
153 telencephalon, where RGCs reside (**Figure 3C, C'; E, E'; G, G'**, and **Table 2**). To
154 determine if EGFP transgene expression accurately reflects endogenous *mdka*
155 expression, we compared it with endogenous *mdka* expression at single-cell resolution
156 (**Figure 3H-J**). In CRE2, CRE4 and CRE6 transgenic lines, EGFP-positive cells were
157 present along the VZ with endogenous *mdka*-positive RGCs (**Figure 3H-J''**).
158 Quantification of confocal stack images showed that roughly half of *mdka*-positive
159 RGCs co-expressed EGFP in each CRE transgenic lines, with no significant difference
160 among the three CRE lines (**Figure 3K**). In the CRE6 transgenic line, EGFP
161 expression was also observed outside of VZ, where endogenous *mdka* is not
162 expressed, suggesting that CRE6 activity leads to ectopic transgene expression
163 (**Figure 3J''**, white arrows). Since we previously reported that *mdka* expression is
164 predominant in quiescent RGCs compared to activated RGCs [21], we next
165 exanimated whether CRE2, CRE4 and CRE6 drive EGFP expression in similar
166 manner. To investigate this, we analyzed the expression of the RGC marker S100β
167 and the proliferation marker PCNA in EGFP-positive cells of each CRE transgenic line
168 (**Figure 3L**). All CRE transgenic lines exhibited robust EGFP expression, primarily in

169 quiescent type 1 RGCs marked by S100β+/PCNA−, closely resembling the
170 endogenous *mdka* expression (**Figure 3M; Figure S1C; Figure S3A-A'''**, **B-B'''**).
171 Although each CRE captured specific aspects of endogenous *mdka* expression, none
172 of them alone fully recapitulated its complete spatial pattern in the adult telencephalon.
173 A similar discrepancy was observed during embryonic development at 24 hpf (**Figure**
174 **2**). While *Tg(CRE2-gata2aPR:EGFP)*, *Tg(CRE4-gata2aPR:EGFP)*, and *Tg(CRE6-*
175 *gata2aPR:EGFP)* each reflect certain aspects of *mdka* expression, their activity was
176 incomplete in both spatial distribution and intensity. Interestingly, CREs that were
177 strongly active in embryonic central nervous system (**Figure 2C**, **C'**) also exhibited
178 activity in the adult telencephalon (**Figure 3C, E and G**). However, their expression
179 patterns differed from that of the endogenous *mdka* mRNA, suggesting that distinct
180 regulatory elements control *mdka* expression at different developmental stages.
181 These findings indicate that full *mdka* expression likely requires a combination of
182 multiple CREs, and that these combinations may vary between embryonic and adult
183 stages, particularly in the adult telencephalon.

184 **Identification of injury-responsive CREs regulating *mdka* expression in the adult**
185 **telencephalon**

186 Since *mdka* expression is significantly upregulated during telencephalon regeneration
187 following brain injury, particularly in type 1 RGCs [21], we subjected all six *mdka* CRE
188 transgenic lines to telencephalon injury (**Figure 4B-G, B'-G'**). All injury-related
189 analyses were performed at 5 days post-lesion (dpl), based on prior RNA-sequencing
190 and RT-qPCR data showing that *mdka* expression peaks at this time point in the
191 injured hemisphere, with a 1.37-fold increase compared to the uninjured side ($p = 2.68$
192 $\times 10^{-9}$) [21]. This time point therefore provided an optimal window to evaluate injury-
193 induced regulatory activity of the CREs. The injury was induced in the right hemisphere
194 using a 30G syringe needle inserted through the skull [27, 43], while the uninjured
195 contralateral hemisphere served as an internal control (**Figure 4A**). Following injury,
196 EGFP reporter expression remained absent in the VZ of the Dm region in transgenic
197 lines carrying CRE1, CRE3, and CRE5 (**Figure 4B, B', D, D', F,** and **F'**), consistent
198 with the lack of expression observed under homeostatic conditions (**Figure 3B, B', D,**
199 **D', F,** and **F'**). In contrast, transgenic lines with CRE2 (**Figure 4C, C'**), CRE4 (**Figure**
200 **4E, E'**), and CRE6 (**Figure 4G, G'**) showed EGFP expression in the Dm of the VZ.

201 However, for all three CREs, the number of EGFP-positive RGCs in the injured
202 hemisphere remained largely unchanged compared to the uninjured contralateral side,
203 with no significant differences between the CREs (**Figure 4H**). Assessment of RGC
204 stemness, based on the proportion of type 1 RGCs among EGFP-positive cells,
205 revealed differences between CREs in the injured (ipsilateral) brain hemisphere.
206 Specifically, CRE2 showed a significantly higher proportion of quiescent type 1 RGCs
207 compared to CRE6 (**Figure 4I**, $p < 0.01$). In contrast, on the contralateral (uninjured)
208 side, approximately three-quarters of EGFP-positive RGCs remained quiescent
209 across all CRE lines, consistent with the proportions observed under homeostatic
210 conditions (**Figure 3M; Figure 4I**). These results suggest that none of the individual
211 CREs contain a strongly injury-responsive regulatory element sufficient to upregulate
212 *mdka* expression during regeneration. Similar to the regulation observed under
213 physiological conditions, it is likely that multiple CREs must act in combination to
214 mediate a full regenerative response.

215 **Cooperative CRE activity enhances faithful transgene expression in embryos,**
216 **adult RGCs, and in response to injury**

217 Analysis of individual stable transgenic lines showed that none of the six CREs alone
218 fully recapitulated the spatial expression pattern of *mdka* throughout embryonic
219 development and adulthood, under either homeostatic or regenerative conditions. To
220 investigate potential cooperative interactions among these CREs, we generated a
221 combined CRE2346 transgenic reporter construct (**Figure 5A**). This construct
222 integrates CRE3, which showed strong regulatory activity during embryogenesis,
223 together with CRE2, CRE4, and CRE6, which were effective in the adult
224 telencephalon. Under homeostatic conditions, the CRE2346 construct drove EGFP
225 expression patterns that closely mimicked endogenous *mdka* expression in embryos
226 (**Figure 5B-B''**). In the adult telencephalon (**Figure 5C, D-D''**), CRE2346 mediated
227 specific EGFP expression in the Dm of the VZ (white arrowheads, **Figure 5D'**),
228 displaying RGC morphology and co-expression with the RGC marker S100β.
229 Transgene fidelity assessment revealed that CRE2346 was active in the majority
230 (median 88%) of *mdka*-positive RGCs, demonstrating significantly higher coverage
231 than any individual CRE (**Figure 5E**). However, analysis of RGC stemness, assessed

232 by immunolabeling for PCNA and S100β, showed no significant effect of the CRE
233 combination (**Figure 5F-F'''**, **G**).

234 We next investigated how the combination of *mdka* cis-regulatory elements (CREs)
235 influences transgene expression during regenerative neurogenesis following brain
236 injury (**Figure 6**). After stab injury, EGFP expression driven by the CRE2346 construct
237 was observed in the ventricular zone (VZ) of both the injured (ipsilateral) and uninjured
238 (contralateral) hemispheres, closely mirroring the endogenous *mdka* expression
239 pattern (**Figure 6A, B-B''**). Notably, injury-induced *mdka* upregulation at the lesion
240 site, which occurs outside the VZ, was also faithfully reproduced by the CRE2346 line
241 (**Figure 6C-C''**). Quantification revealed that the number of radial glial cells (RGCs)
242 expressing EGFP in the injured hemisphere was comparable to that in the
243 contralateral side across all CRE lines, further reflecting endogenous *mdka* expression
244 (**Figure 6D**). Moreover, EGFP intensity was significantly increased in the injured
245 hemisphere in the CRE2346 line ($p < 0.001$), aligning with our prior observations of
246 injury-induced *mdka* upregulation (**Figure 6E**) [21]. To evaluate the impact of
247 combining CREs, we compared transgene fidelity and ectopic expression between
248 CRE2346 and single CRE lines (**Figure 6F-G**). The combination significantly improved
249 transgene fidelity, with consistent expression levels between ipsilateral and
250 contralateral hemispheres (**Figure 6F**). Additionally, CRE2346 effectively suppressed
251 the ectopic, off-target expression seen with CRE4 and CRE6 alone, which had
252 previously shown high levels of non-specific activity (**Figure 6G**). We then assessed
253 whether the CRE combination preserved the identity and stemness of transgene-
254 expressing RGCs. Co-immunolabeling with S100β and PCNA allowed us to
255 distinguish quiescent (type 1) from activated (type 2) RGCs (**Figure 6H-I'''**). In the
256 uninjured (contralateral) hemisphere, CRE2346 increased the proportion of EGFP+
257 quiescent RGCs to 84%, closely approaching the 94% observed for endogenous *mdka*
258 expression (**Figure 6J**). However, in the injured hemisphere, this fidelity was reduced.
259 All constructs, including CRE2346, showed a marked decrease in the proportion of
260 quiescent RGCs (39-69%), significantly lower than the 90% observed with
261 endogenous *mdka*. This suggests that although the CRE2346 line closely replicates
262 endogenous *mdka* activity under normal conditions and partially during regeneration,
263 it likely lacks additional regulatory elements necessary for fully recapitulating *mdka*'s
264 injury response, particularly for maintaining the quiescent RGC state.

265 In summary, our findings demonstrate that the CRE2346 combination effectively
266 drives *mdka*-like EGFP expression in RGCs with high spatial specificity and
267 responsiveness to injury (**Table 3**). This highlights the necessity of multiple regulatory
268 elements for precise spatial and temporal control of *mdka* expression under both
269 physiological and regenerative conditions. Interestingly, all four CREs contain multiple
270 transcription factor binding sites, including robust AP-1 binding sites within their
271 evolutionarily conserved regions (**Figure S5**). AP-1 is a well-known regulator of gene
272 expression during regeneration across various tissues and species, including the
273 zebrafish heart, fin, and tail [35, 44-48], supporting the potential role of these CREs in
274 the regenerative response to injury.

275 **Discussion**

276 Our study reveals that *mdka* expression in the zebrafish central nervous system is
277 regulated by a complex and highly context-dependent network of CREs. These
278 elements act in a modular, combinatorial, and sometimes redundant fashion, reflecting
279 a multifaceted regulatory architecture that governs *mdka* transcription across different
280 developmental stages and physiological states. Consistent with previous reports,
281 *mdka* displays dynamic, tissue-specific expression patterns. For example, in the adult
282 zebrafish telencephalon, *mdka* is expressed in RGCs under homeostatic conditions
283 [21], while in the retina, it is absent in resting stem cells but becomes induced in
284 proliferating Müller glia following injury [29, 49]. Interestingly, in the injured
285 telencephalon, *mdka* expression remains restricted to quiescent RGCs, underscoring
286 its tight, tissue-specific transcriptional control [21].

287 **Modular and context-specific regulation of *mdka***

288 Our transgenic analyses demonstrate that *mdka* expression is orchestrated by multiple
289 CREs, each contributing distinct spatiotemporal aspects to its regulatory program.
290 Some elements, such as CRE5 and CRE3, are active primarily during embryogenesis.
291 For example, CRE3 drives strong expression in the embryonic brain and spinal cord
292 but fails to recapitulate specific adult brain patterns, instead causing ectopic and
293 nonspecific activation (**Table 3**). In contrast, elements like CRE2 are active mainly in
294 the adult telencephalon, particularly in RGCs located in the Dm of the VZ. This
295 modularity is not limited to the brain. In the heart, previous studies showed that a
296 transgene containing *mdka* intronic sequences (*mdka*_e2, overlapping our CRE3,
297 **Table S1**) was active in the developing epicardium but inactive after adult injury [35].
298 Meanwhile, a downstream element (*mdka*_e2, overlapping CRE6, **Table S1**) was
299 inactive during development but became induced in a subset of adult epicardial cells
300 following injury [35]. These examples reinforce the idea that distinct CREs mediate
301 *mdka* expression in different developmental or physiological contexts.

302 **Combinatorial input cooperative and redundant CRE activity**

303 While individual CREs contribute to specific features of *mdka* expression, none alone
304 were sufficient to fully recapitulate endogenous expression, particularly in response to

305 injury. For instance, CRE2, CRE4, and CRE6 each drove weak expression in adult
306 telencephalic RGCs, but none showed injury responsiveness on their own. However,
307 when combined in a multi-CREs construct, these same elements collectively drove
308 expression that closely mimicked endogenous *mdka*, including robust injury-induced
309 activation. This supports a model in which full *mdka* expression depends on the
310 cooperative action of multiple CREs. Such combinatorial regulation may reflect the
311 integration of distinct signaling inputs across separate regulatory elements. One
312 possibility is that different signaling pathways act through specific CREs, with their
313 additive or synergistic activity required to achieve the proper spatiotemporal
314 expression profile. In this context, the effects of different CREs may be additive
315 meaning that multiple enhancers with similar expression patterns together drive
316 expression to levels that individual elements cannot reach on their own. Alternatively,
317 or additionally, a single signaling pathway might act on multiple CREs in parallel, with
318 full activation only occurring when all responsive elements are engaged. This
319 combinatorial strategy may also contribute to enhanced specificity by limiting enhancer
320 activity to overlapping spatial domains, thereby reducing ectopic expression. The
321 presence of conserved AP-1 binding motifs within CRE2, CRE3, CRE4, and CRE6
322 (**Figure S5A-D**), coupled with the established role of the AP-1 complex in regeneration
323 [34, 44, 47], supports both scenarios. Importantly, our observations also reveal
324 redundancy among CREs. Although each element has specific functions, some show
325 overlapping activity. For instance, despite weak individual responses to injury, CRE2,
326 CRE4, and CRE6 all target the same VZ region. Furthermore, CRISPR/Cas9-
327 mediated deletion of a regulatory element in the regenerating fin did not abolish *mdka*
328 expression, and regeneration proceeded without detectable patterning defects [34].
329 This suggests that redundant or compensatory enhancer activity may preserve gene
330 expression when individual elements are disrupted. Such redundancy adds
331 robustness to the regulatory system, ensuring consistent *mdka* activation even in
332 fluctuating or damaged environments. Together, our results highlight a regulatory logic
333 in which enhancer modularity, cooperation, and redundancy work in concert to control
334 *mdka* expression with high precision and resilience.

335 **Broader implications for gene regulation and regenerative biology**

336 The modular and distributed regulatory architecture of *mdka* is consistent with
337 classical models of enhancer function. The *even-skipped (eve)* gene in *Drosophila*, for
338 example, is expressed in a seven-stripe pattern during embryogenesis, with each
339 stripe controlled by a separate enhancer integrating local signals [50, 51]. Similarly, in
340 mammals, the neural crest gene *sox10* is regulated by multiple enhancers with
341 overlapping and redundant functions, enabling robust expression across tissues and
342 stages [52, 53]. These cases, like *mdka*, illustrate how enhancer modularity enables
343 nuanced, context-dependent expression and buffering against perturbation. Our *mdka*
344 reporter lines provide a useful system for dissecting transcriptional programs that
345 govern adult neurogenesis and injury-induced gene activation. These tools could be
346 employed to identify upstream regulators of regenerative gene expression and screen
347 for factors that modulate regenerative capacity *in vivo*.

348 **Regulatory complexity vs. simplicity: A comparative perspective**

349 Intriguingly, the complexity of *mdka* regulation contrasts with the simpler enhancer
350 architecture observed for other genes expressed in the same cellular context. For
351 example, *id1*, which is co-expressed with *mdka* in quiescent RGCs under both
352 physiological and regenerative conditions, appears to be controlled by a single
353 enhancer responsive primarily to BMP signaling [24, 25]. Despite their overlapping
354 expression domains, *id1* and *mdka* rely on very different regulatory strategies. This
355 contrast raises important questions: Why do some genes require complex enhancer
356 networks while others are regulated through simpler mechanisms? Comparative
357 studies between genes like *mdka* and *id1* could illuminate how enhancer complexity
358 evolves and functions in the context of regeneration and plasticity.

359 **Limitations and future directions in defining the *mdka* regulatory landscape**

360 Our primary goal was to identify and functionally validate CREs that positively regulate
361 *mdka* expression. Using *in vivo* transgenesis in zebrafish embryos and adults, we
362 discovered several elements that drive EGFP expression in patterns consistent with
363 endogenous *mdka* activity. These findings provide a foundation for understanding how
364 *mdka* is regulated during development and regeneration. However, a key limitation of
365 our approach is that it is optimized to detect enhancer activity and does not capture
366 negative regulatory elements such as silencers. Traditional reporter assays are unable

367 to distinguish between a lack of enhancer function and active repression. For instance,
368 CRE1 did not drive detectable EGFP expression on its own, but whether this indicates
369 silencer activity or simply absence of regulatory function remains unresolved. To
370 address this, future studies should explore combinatorial testing, such as integrating
371 CRE1 with active enhancers like CRE2346, to determine if it can restrict or suppress
372 ectopic expression. Such designs could uncover context-dependent repression that
373 would remain hidden when elements are tested in isolation. Our data also underscore
374 the modular nature of the *mdka* regulatory architecture, which involves synergy,
375 additivity, and redundancy among CREs. Additive effects, where multiple elements
376 with overlapping activity are needed to achieve full expression, should be
377 distinguished from redundancy, where one CRE can compensate for the absence of
378 another. Both features likely contribute to the robustness and precision of *mdka*
379 expression in both physiological and regenerative contexts. A fuller understanding of
380 this regulatory logic will require experimental strategies that can reveal both positive
381 and negative regulatory interactions.

382 Another limitation relates to the use of fluorescent reporter systems. The relative
383 stability of EGFP protein may result in prolonged signal even after *mdka* mRNA
384 expression has subsided, potentially contributing to discrepancies in spatial
385 localization. To address this, we performed *in situ* hybridization for *egfp* mRNA, which
386 confirmed both expected expression in the dorsomedial region and ectopic expression
387 in the parenchyma (data not shown). These findings further support the idea that
388 certain silencer elements may be absent from our current constructs. Given its lack of
389 activity in isolation, CRE1 remains a strong candidate for a negative regulatory
390 element, and its function in combination with other enhancers will be a priority for future
391 studies. In addition, mRNA-level analysis across multiple transgenic lines will be
392 essential for identifying those that most accurately recapitulate endogenous *mdka*
393 expression in radial glial cells. Collectively, these insights highlight the importance of
394 both enhancer and silencer elements in shaping the spatial and temporal dynamics of
395 *mdka* regulation under homeostatic and regenerative conditions.

396

397 **Materials and methods**

398 **Zebrafish husbandry**

399 All zebrafish lines were maintained at the European Zebrafish Resource Center
400 (EZRC). Experiments were performed on 6- to 12-month-old wild-type fish or
401 transgenic reporter lines (**Table S2**). Animal husbandry was carried out in accordance
402 with permit guidelines under §11 TSchG (Regierungspräsidium Karlsruhe,
403 Aktenzeichen 35–9185.64/BH KIT). Fish were kept according to the European Society
404 for Fish Models in Biology and Medicine (EuFishBioMed) guidelines at the Karlsruhe
405 Institute of Technology (KIT) [54], and animal experimentation adhered to German
406 animal protection standards, approved by the Government of Baden-Württemberg
407 (Regierungspräsidium Karlsruhe, Reference Numbers: 35-9185.81/G-214/21 and 35-
408 9185.81/G-215/21). Efforts were made to minimize animal distress and reduce their
409 number.

410 **Plasmids construction**

411 Plasmids for enhancer/promoter reporter assays were generated using Gateway
412 cloning and TOPO/TA cloning strategies. The primers used for PCR amplification of
413 putative CREs, and promoter are listed in **Table S3,** while the coordinates and sizes
414 of the CREs and the promoter are provided in **Table S1**. Most plasmids (**Table S4**)
415 were constructed using commonly available vectors, with detailed protocols for
416 Gateway cloning available as described in Kwan et al., 2007 [55]. The pTol2-
417 mdkaCRE2346-gata2aPR:egfp-pA plasmid was created by combining four *mdka*
418 putative CREs (CRE2, CRE3, CRE4, and CRE6) into the pT2KHGPzGATA2C1
419 destination vector and was synthesized by GenScript Biotech Corporation.

420 **Microinjection to generate transient and stable transgenesis**

421 One-cell stage embryos were injected with 1 µl of 20 ng/µl Tol2 transposase mRNA,
422 1 µl of 10 % phenol red, 50 ng/µl plasmid DNA, and nuclease-free water (final volume
423 10 µl) directly into the yolk through the chorion. After injection, embryos were
424 incubated at 28 °C in E3 medium with methylene blue. At 24 hpf, embryos were sorted
425 based on EGFP fluorescence. Positive F0 founders were identified by EGFP

426 expression, raised to sexual maturity, and outcrossed with wildtype zebrafish. Stable
427 EGFP expression in ~20 % of F1 progeny confirmed successful stable transgenesis.

428 **Fluorescent *in situ* hybridization (FISH) of whole-mount embryos**

429 Embryos were collected at the desired developmental stage, and chorions were
430 removed manually or with pronase (1:100 w/v, 28.5 °C). The *mdka* probe (Molecular
431 Instruments Inc.) was used, following the HCR™ RNA-FISH protocol with minor
432 modifications, available on the Molecular Instruments website.

433 **Stab injury of adult telencephalon and preparation of sections**

434 The stab injury experiment and telencephalon sections were performed following the
435 protocol described by Schmidt et al. [43].

436 **FISH on adult telencephalon sections and embryos**

437 For experiments using probes from Molecular Instruments Inc., the protocol "HCR™
438 RNA-FISH protocol for fresh frozen or fixed frozen tissue sections was followed, with
439 minor modifications. Specifically, for 24 hpf embryos, proteinase K treatment was
440 conducted at a concentration of 10 µg/ml (diluted from a 1000 × stock to 1 × working
441 concentration) for 10 min to improve probe penetration. The *mdka* probe used for
442 fluorescent *in situ* hybridization was purchased from the Molecular Instruments Inc.
443 with a dilution of 1:500.

444 **Immunohistochemistry (IHC) on adult telencephalon sections**

445 Vibratome sections were blocked with 1 ml blocking buffer for 1 hour at RT. After
446 removing the buffer, sections were incubated overnight at 4 °C with primary antibodies
447 in 300 µl blocking buffer. The next day, sections were washed 3 × 10 min with PTW (1
448 × PBS containing 0.1% Tween-20), then incubated with secondary antibodies (diluted
449 in PTW) for 2 hours at RT in the dark. DAPI staining (1:2000 in PTW) was performed
450 for 20 min if needed, followed by 3 × 5 min washes in PTW. Sections were mounted
451 and imaged. All antibodies used are listed in **Table S5**.

452 **Mounting for imaging**

453 For embryos, dechorionated embryos were embedded in a 1.6 % low melting-point
454 agarose (Sigma) and 0.016 % Tricaine (Sigma) mixture in E3 medium, oriented within
455 1 min using a needle or fine hair, left at room temperature for 3 min, cooled at 4 °C for
456 3 min, supplemented with water drops to prevent evaporation. While for adult
457 telencephalon sections, fluorescently labelled brain sections were mounted on glass
458 slides with 0.17 mm coverslips using Aqua Polymount (PolySciences Inc., USA) and
459 stored at 4 °C in the dark before and after imaging [43].

460 **Confocal imaging**

461 Fluorescently labelled embryos and telencephalon sections were imaged using Leica
462 TCS SP5 DM5000 and SP8/DLS confocal fluorescence microscope (Leica
463 Microsystems, Wetzlar, Germany) equipped with 405 nm, 488 nm, 561 nm and 633
464 nm lasers. Excitation (Ex) wavelengths and emission (Em) ranges were as follows: Ex
465 488 nm for AlexaFluor 488 (EGFP, Em 492-550 nm), Ex 561 nm for AlexaFluor 561
466 (PCNA, Em 565-605 nm), Ex 633 nm for AlexaFluor 633 (S100β, Em 650-740 nm),
467 Ex 633 nm for AlexaFluor 633-labeled *mdka* RNA probe (EM 655-724 nm), and Ex
468 405 nm for DAPI (Em 409-480 nm). Imaging was performed with sequential scanning
469 at 16-bit color depth with a 1.0 AU pinhole aperture. Images were acquired at a
470 resolution of 1024 × 1024-pixel resolution, with a pixel size of approximately 1.55 μm
471 × 1.55 μm (field of view: ~1.55 mm × 1.55 mm), using a 63 ×/1.20 NA Water Immersion
472 objective (Leica Microsystems) at a scanning frequency of 400 Hz. Laser intensity,
473 PMT gain, detector settings, AOTF (Acousto-Optic Tuneable Filters) attenuation and
474 other imaging settings were kept constant across experimental groups to ensure
475 comparability.

476 **Image processing and arrangement**

477 Images were processed with consistent exposure times and gain settings across all
478 series. Z-stack maximum projections were generated and cropping or rotation was
479 performed in ImageJ/Fiji. For wide-field images in **Figure S2**, deconvolution using the
480 Iterative Deconvolve 3D and Diffraction PSF 3D plugins were applied to remove out-
481 of-focus blur and enhance clarity. All figures, including flowcharts, were created and
482 arranged using Microsoft PowerPoint (version 16.78) or Adobe Illustrator 2022
483 (version 26.4.1).

Statistical analysis

Three sections per brain were analyzed from at least three individuals (with sample sizes indicated in the figure legends). Each brain section was treated as a single data point. All statistical analyses were performed and visualized using R. To determine the appropriate statistical test, data normality was assessed using the *Shapiro–Wilk* test with a significance level of $\alpha = 0.05$. For normally distributed data, parametric tests were used: the *Welch t*-test for comparisons between two samples, and the *Tukey HSD* test following a significant *ANOVA* ($\alpha = 0.05$) for comparisons involving more than two groups. For non-normally distributed data, the *Mann–Whitney U* test was used for unpaired two-sample comparisons, and the *Dunn* test was applied following a significant *Kruskal–Wallis* rank sum test ($\alpha = 0.05$) for multiple-group comparisons.

Acknowledgements

We would like to sincerely thank Anne Schröck for her invaluable technical support throughout this project. We are grateful to Luisa Lübke, Gaoqun Zhang, and Barbara Schornick for their contributions during the early phase of this study, and to Fushun Chen for his initial support with bioinformatics. We also thank Ferenc Müller and Yavor Hadzhiev for their helpful discussions and advice on bioinformatics approaches. Research in Sepand Rastegar's laboratory is supported by the BioInterfaces in Technology and Medicine and Natural, Artificial, and Cognitive Information Processing (NACIP) programmes of the Helmholtz Association, as well as by project grants from the German Research Foundation (DFG GRK2039, STR 439/17-1, RA 3469/5-1) and the Marie Skłodowska-Curie Initial Training Networks (ITNs) ZenCode and Danio-Recode. Jincan Chen is supported by a grant from the China Scholarship Council (CSC), grant number 202106310017. We thank the KIT Publication Fund of the Karlsruhe Institute of Technology for its support. Open access funding was enabled and organized by Projekt DEAL.

Conflict of interest

The authors declare no conflict of interest.

Author contributions

SR designed, supervised the experiments, analysed the data, and co-wrote the manuscript with JC, MT and ND. JC, AH, MT and TB conducted experiments and analysed data. JC and MT analysed and quantified the data. CV conducted the Hi-C and 4C data analysis. All authors have reviewed and approved the final version of the manuscript for publication.

Data availability statement

The data that supports the findings of this study are available in the main text and the supporting information of this article.

References

1. Chen, J. C., Sanchez-Iranzo, H., Diotel, N. & Rastegar, S. (2024) Comparative insight into the regenerative mechanisms of the adult brain in zebrafish and mouse: highlighting the importance of the immune system and inflammation in successful regeneration, *Febs Journal.* **291**, 4193-4205.

2. Marques, I. J., Lupi, E. & Mercader, N. (2019) Model systems for regeneration: zebrafish, *Development.* **146**.

3. Becker, T. & Becker, C. G. (2022) Regenerative neurogenesis: the integration of developmental physiological and immune signals, *Development.* **149**.

4. Gemberling, M., Bailey, T. J., Hyde, D. R. & Poss, K. D. (2013) The zebrafish as a model for complex tissue regeneration, *Trends Genet.* **29**, 611-620.

5. Kizil, C., Kaslin, J., Kroehne, V. & Brand, M. (2012) Adult neurogenesis and brain regeneration in zebrafish, *Dev Neurobiol.* **72**, 429-461.

6. Alunni, A. & Bally-Cuif, L. (2016) A comparative view of regenerative neurogenesis in vertebrates, *Development.* **143**, 741-753.

7. Howe, K.Clark, M. D.Torroja, C. F.Torrance, J.Berthelot, C.Muffato, M.Collins, J. E.Humphray, S.McLaren, K.Matthews, L.McLaren, S.Sealy, I.Caccamo, M.Churcher, C.Scott, C.Barrett, J. C.Koch, R.Rauch, G. J.White, S.Chow, W.Kilian, B.Quintais, L. T.Guerra-Assunçao, J. A.Zhou, Y.Gu, Y.Yen, J.Vogel, J. H.Eyre, T.Redmond, S.Banerjee, R.Chi, J. X.Fu, B. Y.Langley, E.Maguire, S. F.Laird, G. K.Lloyd, D.Kenyon, E.Donaldson, S.Sehra, H.Almeida-King, J.Loveland, J.Trevanion, S.Jones, M.Quail, M.Willey, D.Hunt, A.Burton, J.Sims, S.McLay, K.Plumb, B.Davis, J.Clee, C.Oliver, K.Clark, R.Riddle, C.Eliott, D.Threadgold, G.Harden, G.Ware, D.Mortimer, B.Kerry, G.Heath, P.Phillimore, B.Tracey, A.Corby, N.Dunn, M.Johnson, C.Wood, J.Clark, S.Pelan, S.Griffiths, G.Smith, M.Glithero, R.Howden, P.Barker, N.Stevens, C.Harley, J.Holt, K.Panagiotidis, G.Lovell, J.Beasley, H.Henderson, C.Gordon, D.Auger, K.Wright, D.Collins, J.Raisen, C.Dyer, L.Leung, K.Robertson, L.Ambridge, K.Leongamornlert, D.McGuire, S.Gilderthorp, R.Griffiths, C.Manthravadi, D.Nichol, S.Barker, G.Whitehead, S.Kay, M., et al. (2013) The zebrafish reference genome sequence and its relationship to the human genome, *Nature.* **496**, 498-503.

8. Driever, W., SolnicaKrezel, L., Schier, A. F., Neuhauss, S. C. F., Malicki, J., Stemple, D. L., Stainier, D. Y. R., Zwartkruis, F., Abdelilah, S., Rangini, Z., Belak, J. & Boggs, C. (1996) A genetic screen for mutations affecting embryogenesis in zebrafish, *Development.* **123**, 37-46.

9. Ellingsen, S., Laplante, M. A., König, M., Kikuta, H., Furmanek, T., Hoivik, E. A. & Becker, T. S. (2005) Large-scale enhancer detection in the zebrafish genome, *Development.* **132**, 3799-3811.

10. Choe, C. P., Choi, S. Y., Kee, Y., Kim, M. J., Kim, S. H., Lee, Y., Park, H. C. & Ro, H. (2021) Transgenic fluorescent zebrafish lines that have revolutionized biomedical research, *Lab Anim Res.* **37**, 26.

11. Parinov, S., Kondrichin, I., Korzh, V. & Emelyanov, A. (2004) Tol2 transposon-mediated enhancer trap to identify developmentally regulated zebrafish genes in vivo, *Dev Dyn.* **231**, 449-59.

12. Hörtenhuber, M., Mukarram, A. K., Stoiber, M. H., Brown, J. B. & Daub, C. O. (2020) *-DCC: A platform to collect, annotate, and explore a large variety of sequencing experiments, *Gigascience.* **9**.

13. Yang, H., Luan, Y., Liu, T., Lee, H. J., Fang, L., Wang, Y., Wang, X., Zhang, B., Jin, Q., Ang, K. C., Xing, X., Wang, J., Xu, J., Song, F., Sriranga, I., Khunsriraksakul, C., Salameh, T., Li, D., Choudhary, M. N. K., Topczewski, J., Wang, K., Gerhard, G. S., Hardison, R. C., Wang, T., Cheng, K. C. & Yue, F. (2020) A map of cis-regulatory elements and 3D genome structures in zebrafish, *Nature.* **588**, 337-343.

14. Baranasic, D., Hörtenhuber, M., Balwierz, P. J., Zehnder, T., Mukarram, A. K., Nepal, C., Várnai, C., Hadzhiev, Y., Jimenez-Gonzalez, A., Li, N., Wragg, J., D'Orazio, F. M., Relic, D., Pachkov, M., Díaz, N., Hernández-Rodríguez, B., Chen, Z. L., Stoiber, M., Dong, M., Stevens, I., Ross, S. E., Eagle, A., Martin, R., Obasaju, O., Rastegar, S., McGarvey, A. C., Kopp, W., Chambers, E., Wang, D., Kim, H. R., Acemel, R. D., Naranjo, S., Lapinski, M., Chong, V., Mathavan, S., Peers, B., Sauka-Spengler, T., Vingron, M., Carninci, P., Ohler, U., Lacadie, S. A., Burgess, S. M., Winata, C., van Eeden, F., Vaquerizas, J. M., Gómez-Skarmeta, J. L., Onichtchouk, D., Brown, B., Bogdanovic, O., van Nimwegen, E., Westerfield, M., Wardle, F. C., Daub, C. O., Lenhard, B. & Müller, F. (2022) Multiomic atlas with functional stratification and developmental dynamics of zebrafish regulatory elements, *Nat Genet.* **54**, 1037-1050.

15. Diotel, N., Lübke, L., Strähle, U. & Rastegar, S. (2020) Common and distinct features of adult neurogenesis and regeneration in the telencephalon of zebrafish and mammals, *Front Neurosci-Switz.* **14**.

16. Ghaddar, B., Lübke, L., Couret, D., Rastegar, S. & Diotel, N. (2021) Cellular mechanisms participating in brain repair of adult zebrafish and mammals after injury, *Cells-Basel.* **10**.

17. Rodriguez Viales, R., Diotel, N., Ferg, M., Armant, O., Eich, J., Alunni, A., März, M., Bally-Cuif, L., Rastegar, S. & Strahle, U. (2015) The helix-loop-helix protein Id1 controls stem cell proliferation during regenerative neurogenesis in the adult zebrafish telencephalon, *Stem Cells.* **33**, 892-903.

18. Demirci, Y., Cucun, G., Poyraz, Y. K., Mohammed, S., Heger, G., Papatheodorou, I. & Ozhan, G. (2020) Comparative Transcriptome Analysis of the Regenerating Zebrafish Telencephalon Unravels a Resource With Key Pathways During Two Early Stages and Activation of Wnt/beta-Catenin Signaling at the Early Wound Healing Stage, *Front Cell Dev Biol.* **8**, 584604.

19. Gourain, V., Armant, O., Lubke, L., Diotel, N., Rastegar, S. & Strahle, U. (2021) Multi-Dimensional Transcriptome Analysis Reveals Modulation of Cholesterol Metabolism as Highly Integrated Response to Brain Injury, *Front Neurosci.* **15**, 671249.

609 20. Lange, C., Rost, F., Machate, A., Reinhardt, S., Lesche, M., Weber, A., Kuscha,
610 V., Dahl, A., Rulands, S. & Brand, M. (2020) Single cell sequencing of radial glia
611 progeny reveals the diversity of newborn neurons in the adult zebrafish brain,
612 *Development.* **147**.

613 21. Lübke, L., Zhang, G. Q., Straehle, U. & Rastegar, S. (2022) *mdka* expression is
614 associated with quiescent neural stem cells during constitutive and reactive
615 neurogenesis in the adult zebrafish telencephalon, *Brain Sci.* **12**.

616 22. Winkler, C. & Yao, S. (2014) The midkine family of growth factors: diverse roles in
617 nervous system formation and maintenance, *Br J Pharmacol.* **171**, 905-12.

618 23. Aynacioglu, A. S., Bilir, A. & Tuna, M. Y. (2019) Involvement of midkine in
619 autoimmune and autoinflammatory diseases, *Mod Rheumatol.* **29**, 567-571.

620 24. Zhang, G. Q., Lübke, L., Chen, F. S., Beil, T., Takamiya, M., Diotel, N., Strähle, U.
621 & Rastegar, S. (2021) Neuron-radial glial cell communication via BMP/Id1 signaling is
622 key to long-term maintenance of the regenerative capacity of the adult zebrafish
623 telencephalon, *Cells-Basel.* **10**.

624 25. Zhang, G. Q., Ferg, M., Lübke, L., Takamiya, M., Beil, T., Gourain, V., Diotel, N.,
625 Strähle, U. & Rastegar, S. (2020) Bone morphogenetic protein signaling regulates Id1-
626 mediated neural stem cell quiescence in the adult zebrafish brain via a
627 phylogenetically conserved enhancer module, *Stem Cells.* **38**, 875-889.

628 26. Adolf, B., Chapouton, P., Lam, C. S., Topp, S., Tannhäuser, B., Strähle, U., Götz,
629 M. & Bally-Cuif, L. (2006) Conserved and acquired features of adult neurogenesis in
630 the zebrafish telencephalon, *Dev Biol.* **295**, 278-293.

631 27. März, M., Schmidt, R., Rastegar, S. & Strähle, U. (2011) Regenerative response
632 following stab injury in the adult zebrafish telencephalon, *Dev Dynam.* **240**, 2221-2231.

633 28. Grivas, D., Gonzalez-Rajal, A. & de la Pompa, J. L. (2021) Midkine-a regulates
634 the formation of a fibrotic scar during zebrafish heart regeneration, *Front Cell Dev Biol.*
635 **9**, 669439.

636 29. Gramage, E., D'Cruz, T., Taylor, S., Thummel, R. & Hitchcock, P. F. (2015) Midkine-
637 a protein localization in the developing and adult retina of the zebrafish and its function
638 during photoreceptor regeneration, *Plos One.* **10**, e0121789.

639 30. Ang, N. B., Saera-Vila, A., Walsh, C., Hitchcock, P. F., Kahana, A., Thummel, R. &
640 Nagashima, M. (2020) Midkine-a functions as a universal regulator of proliferation
641 during epimorphic regeneration in adult zebrafish, *Plos One.* **15**, e0232308.

642 31. Nagashima, M., D'Cruz, T. S., Danku, A. E., Hesse, D., Sifuentes, C., Raymond,
643 P. A. & Hitchcock, P. F. (2020) Midkine-a is required for cell cycle progression of Müller
644 glia during neuronal regeneration in the vertebrate retina, *J Neurosci.* **40**, 1232-1247.

645 32. Kikuchi-Horie, K., Kawakami, E., Kamata, M., Wada, M., Hu, J. G., Nakagawa, H.,
646 Ohara, K., Watabe, K. & Oyanagi, K. (2004) Distinctive expression of midkine in the
647 repair period of rat brain during neurogenesis: immunohistochemical and
648 immunoelectron microscopic observations, *J Neurosci Res.* **75**, 678-87.

649 33. Lien, C. L., Schebesta, M., Makino, S., Weber, G. J. & Keating, M. T. (2006) Gene
650 expression analysis of zebrafish heart regeneration, *Plos Biol.* **4**, e260.

651 34. Thompson, J. D., Ou, J. H., Lee, N., Shin, K., Cigliola, V., Song, L. Y., Crawford,
652 G. E., Kang, J. S. & Poss, K. D. (2020) Identification and requirements of enhancers
653 that direct gene expression during zebrafish fin regeneration, *Development.* **147**.

654 35. Weinberger, M., Simoes, F. C., Gungoosingh, T., Sauka-Spengler, T. & Riley, P. R.
655 (2024) Distinct epicardial gene regulatory programs drive development and
656 regeneration of the zebrafish heart, *Dev Cell.* **59**, 351-367.

657 36. Winkler, C., Schäfer, M., Duschl, J., Schartl, M. & Volff, J. N. (2003) Functional
658 divergence of two zebrafish midkine growth factors following fish-specific gene
659 duplication, *Genome Res.* **13**, 1067-1081.

660 37. Gonzalez, A. J., Baranasic, D. & Müller, F. (2023) Zebrafish regulatory genomic
661 resources for disease modelling and regeneration, *Dis Model Mech.* **16**.

662 38. Chen, Z. L., Omori, Y., Koren, S., Shirokiya, T., Kuroda, T., Miyamoto, A., Wada,
663 H., Fujiyama, A., Toyoda, A., Zhang, S. Y., Wolfsberg, T. G., Kawakami, K., Phillippy,
664 A. M., Mullikin, J. C., Burgess, S. M. & Prog, N. C. S. (2019) De novo assembly of the
665 goldfish (*Carassius auratus*) genome and the evolution of genes after whole-genome
666 duplication, *Sci Adv.* **5**.

667 39. Meng, A. M., Tang, H., Ong, B. A., Farrell, M. J. & Lin, S. (1997) Promoter analysis
668 in living zebrafish embryos identifies a *cis*-acting motif required for neuronal
669 expression of GATA-2, *P Natl Acad Sci USA.* **94**, 6267-6272.

670 40. Navratilova, P., Fredman, D., Hawkins, T. A., Turner, K., Lenhard, B. & Becker, T.
671 S. (2009) Systematic human/zebrafish comparative identification of *cis*-regulatory
672 activity around vertebrate developmental transcription factor genes, *Dev Biol.* **327**,
673 526-540.

674 41. Rastegar, S., Hess, I., Dickmeis, T., Nicod, J. C., Ertzer, R., Hadzhiev, Y., Thies,
675 W. G., Scherer, G. & Strähle, U. (2008) The words of the regulatory code are arranged
676 in a variable manner in highly conserved enhancers, *Dev Biol.* **318**, 366-377.

677 42. Begeman, I. J., Emery, B., Kurth, A. & Kang, J. S. (2022) Regeneration and
678 developmental enhancers are differentially compatible with minimal promoters, *Dev*
679 *Biol.* **492**, 47-58.

680 43. Schmidt, R., Beil, T., Strähle, U. & Rastegar, S. (2014) Stab wound injury of the
681 zebrafish adult telencephalon: A method to investigate vertebrate brain neurogenesis
682 and regeneration, *Jove-J Vis Exp*.

683 44. Beisaw, A., Kuenne, C., Guenther, S., Dallmann, J., Wu, C. C., Bentsen, M.,
684 Looso, M. & Stainier, D. Y. R. (2020) AP-1 contributes to chromatin accessibility to
685 promote sarcomere disassembly and cardiomyocyte protrusion during zebrafish heart
686 regeneration, *Circ Res.* **126**, 1760-1778.

45. Nakamura, M., Yoshida, H., Takahashi, E., Wlizla, M., Takebayashi-Suzuki, K., Horb, M. & Suzuki, A. (2020) The AP-1 transcription factor JunB functions in Xenopus tail regeneration by positively regulating cell proliferation. **522**, 990-995.

46. Wang, W., Hu, C., Zeng, A., Alegre, D., Hu, D., Gotting, K., Ortega Granillo, A., Wang, Y., Robb, S., Schnittker, R., Zhang, S., Alegre, D., Li, H., Ross, E., Zhang, N., Brunet, A. & Sánchez Alvarado, A. (2020) Changes in regeneration-responsive enhancers shape regenerative capacities in vertebrates, *Science.* **369**, eaaz3090.

47. Tamaki, T., Yoshida, T., Shibata, E., Nishihara, H., Ochi, H. & Kawakami, A. (2023) Splashed E-box and AP-1 motifs cooperatively drive regeneration response and shape regeneration abilities, *Biol Open.* **12**.

48. Dong, Y., Yang, Y., Wang, H., Feng, D., Nist, E., Yapundich, N., Spurlock, B., Craft, M., Qian, L. & Liu, J. (2024) Single-cell chromatin profiling reveals genetic programs activating proregenerative states in nonmyocyte cells, *Sci Adv.* **10**, eadk4694.

49. Gramage, E., Li, J. & Hitchcock, P. (2014) The expression and function of midkine in the vertebrate retina, *Brit J Pharmacol.* **171**, 913-923.

50. Goto, T., Macdonald, P. & Maniatis, T. (1989) Early and late periodic patterns of even skipped expression are controlled by distinct regulatory elements that respond to different spatial cues, *Cell.* **57**, 413-422.

51. Berrocal, A., Lammers, N. C., Garcia, H. G. & Eisen, M. B. (2020) Kinetic sculpting of the seven stripes of the Drosophila even-skipped gene, *Elife.* **9**, e61635.

52. Werner, T., Hammer, A., Wahlbuhl, M., Bösl, M. R. & Wegner, M. (2007) Multiple conserved regulatory elements with overlapping functions determine Sox10 expression in mouse embryogenesis, *Nucleic Acids Res.* **35**, 6526-38.

53. Betancur, P., Bronner-Fraser, M. & Sauka-Spengler, T. (2010) Genomic code for Sox10 activation reveals a key regulatory enhancer for cranial neural crest, *Proc Natl Acad Sci U S A.* **107**, 3570-5.

54. Aleström, P., D'Angelo, L., Midtlyng, P. J., Schorderet, D. F., Schulte-Merker, S., Sohm, F. & Warner, S. (2020) Zebrafish: Housing and husbandry recommendations, *Lab Anim-Uk.* **54**, 213-224.

55. Kwan, K. M., Fujimoto, E., Grabher, C., Mangum, B. D., Hardy, M. E., Campbell, D. S., Parant, J. M., Yost, H. J., Kanki, J. P. & Chien, C. B. (2007) The *Tol*2kit: A multisite gateway-based construction kit for *Tol2* transposon transgenesis constructs, *Dev Dynam.* **236**, 3088-3099.

722 **Table 1. Summary of EGFP expression patterns driven by individual CREs in 24**
723 **hpf embryos.**

	Endogenous	CRE1	CRE2	CRE3	CRE4	CRE5	CRE6
Brain	++	-	+	+	+	+	+
Retina	++	-	+	++	++	+	++
Spinal cord	++	-	+	++	+	+	+
Notochord	+	-	+	-	-	-	-
Fin fold/Tail	++	-	-	++	+	-	+
Somite/Muscle	++	-	+	-	++	-	++

724 Note: -, no detectable expression; +, weak expression; ++, strong expression.

725

726 **Table 2. Summary of EGFP expression patterns driven by individual CREs in the**
727 **adult telencephalon.**

	Endogenous	CRE1	CRE2	CRE3	CRE4	CRE5	CRE6
Dm	++	-	++	-	+	-	+
Dl	++	-	+	+	+	-	+
Dp	+	-	-	++	-	-	-
Vd	+	-	+	-	-	-	-
Vv	+	-	+	-	++	-	-

728 Note: -, no detectable expression; +, weak expression; ++, strong expression.
729 Abbreviations: Dm, dorsomedial pallium; Dp, dorsal pallium; Dl, lateral pallium; VZ,
730 ventricular zone; Vd, dorsal nucleus of ventral telencephalon; Vv, ventral nucleus of
731 ventral telencephalon.

732

733 **Table 3. Summary of EGFP expression patterns observed in distinct *mdka* CRE**
734 **transgenic lines.**

CRE(s)	Activity summary
CRE2	Adult regulatory sequence; active in physiological conditions; best matching *mdka* expression
CRE3	Predominantly active during embryonic development; overlaps with mdka expression; shows ectopic expression in the adult telencephalon in Dp and Dl.
CRE4	Adult regulatory sequence; active in NSCs; does not show a significant response to injury
CRE6	Adult regulatory sequence; active in NSCs with ectopic activity in neurons; no significant response to injury
CRE2346	Recapitulates *mdka* expression; EGFP reporter overlaps with *mdka* mRNA in both embryo and adult; inducible upon injury

735 Note: Dp, dorsal pallium; Dl, lateral pallium; NSCs, neural stem cells.
736

737 **Figure legends**

738 **Figure 1. Identification of potential *mdka* regulatory sequences based on**
739 **embryonic developmental ATAC-seq data.** Snapshot of UCSC genome browser
740 tracks displaying ATAC-seq data from different embryonic developmental stages
741 (Dome, 75%-epiboly, 5-9 somites, Prime-5 and Long-pec) across a 45-kilobase region
742 (chr7: 38,875,000-38,920,000; danRer10 assembly). Green peak profiles represent
743 open chromatin regions identified by ATAC-seq. Color-coded horizontal bars indicate
744 the genomic position of putative regulatory elements based on PADRES (Predicted
745 ATAC-seq-supported developmental regulatory elements): promoters (1_TssA and
746 2_TssA2, blue), enhancers (5_EnhA1, red; 7_EnhWk1, orange), and other elements
747 (e.g., 10_Quies, grey). The grey box highlights six putative *mdka* CREs (CRE1 to
748 CRE6) identified in this study, while the magenta box marks the putative *mdka*
749 promoter region. The relative positions of all CREs are shown in reference to the *mdka*
750 gene and its transcription start site (TSS). PhastCons conservation scores derived
751 from zebrafish-carp genome alignment highlights conserved non-coding regions
752 (CNEs) associated with the *mdka* locus.

753

754 **Figure 2. Stable EGFP transgenic line generated using potential *mdka* CREs. A**,
755 Schematic of the plasmid pTol2-mdkaCREx-gata2aPR:egfp-pA, where CREx
756 represents one of the six putative CREs (CRE1 to CRE6). **B-G**, Stable EGFP reporter
757 expression driven by *mdka* CRE1 (B), CRE2 (C), CRE3 (D), CRE4 (E), CRE5 (F),
758 CRE6 (G) in embryo at 24 hours post-fertilization (hpf). **B'-G'**, Merged images showing
759 *mdka* mRNA (magenta) and EGFP (green) expression in the corresponding CRE
760 transgenic lines. *Tg(CRE3-gata2aPR:EGFP)* embryo exhibited strong co-localization
761 of *mdka* mRNA and EGFP signals in the spinal cord (yellow arrowheads, D, D') and
762 fin fold region (white arrowheads, D, D'). *Tg(CRE4-gata2aPR:EGFP)* and *Tg(CRE6-*
763 *gata2aPR:EGFP)* embryos showed strong activity in the retina (green arrowheads)
764 and brain regions (red arrowheads, E, E', G, G'), respectively. *Tg(CRE1-*
765 *gata2aPR:EGFP)* showed no detectable EGFP expression (B, B'). Scale bar: 200 μm.

766

767 **Figure 3. The *mdka* transgenic lines, CRE2, CRE4 and CRE6, drive radial glial**
768 **EGFP expression in the adult telencephalon during constitutive neurogenesis.**
769 **A**, Schematic illustrating the orientation of transverse sections through the
770 telencephalon, with reference to the location of radial glial cells (RGCs). Dm:

771 dorsomedial pallium; VZ: ventricular zone; RGCs: radial glial cells. **B-G'**, EGFP
772 reporter expression in the adult telencephalon across various *mdka* CRE transgenic
773 lines: CRE1 (B-B'. *n* = 3 brains), CRE2 (C-C', *n* = 4), CRE3 (D-D', *n* = 6), CRE4 (E-E',
774 *n* = 3), CRE5 (F-F', *n* = 4), and CRE6 (G-G', *n* = 3). The location of VZ is indicated on
775 the left hemisphere of CRE1 telencephalon, where EGFP expression is absent (B-B').
776 Rectangles in B-G indicate magnified regions shown in B'-G', respectively. Dashed
777 lines outline the telencephalon contour (B-G). **H-J'',** Magnified transverse views of the
778 Dm region showing EGFP (green) and *mdka* mRNA expression (magenta) in three
779 transgenic lines with radial glial EGFP expression: *Tg(CRE2-gata2aPR:EGFP)*(H-H''),
780 *Tg(CRE4-gata2aPR:EGFP)*(I-I''), and *Tg(CRE6-gata2aPR:EGFP)* (J-J''). White
781 arrowheads highlight RGCs of *mdka* mRNA and EGFP co-localization, reflecting
782 faithful activity of CRE2, CRE4 and CRE6. Arrows in the panel J'' indicate the ectopic
783 EGFP expression of CRE6 located outside of VZ. **K**, The fidelity of CRE2, CRE4 and
784 CRE6 activity was evaluated by quantifying the percentage of EGFP-positive cells
785 among endogenous *mdka*-positive RGCs with the confocal images as shown the
786 panels H-J. Results are shown as boxplots with the median values. No significant
787 difference was observed between different CREs (*ANOVA* test, $p = 0.84$). **L**, S100β+
788 EGFP cells are classified either as type 1 (quiescent, PCNA-negative) or type 2
789 (activated, PCNA-positive) based on PCNA expression. **M**, Quantification of type 1
790 and type 2 RGC population in CRE2, CRE4, and CRE6. The mean ± standard
791 deviation (error bar) of type 1 RGCs is expressed as a percentage of the total RGC
792 population. No significant difference was observed between different CREs (*n.s.*;
793 *Kruskal-Wallis* test, $p = 0.97$). Representative confocal images corresponding to this
794 quantification are provided in Supplementary Figure S3A-A''', B-B''' and Figure S4A-
795 A''', C-C''', showing co-immunostaining for EGFP, S100β, and PCNA. Each data point
796 represents an individual brain slice. Scale bar: 200 μm (B-G), 25 μm (B'-G', H-J) and
797 10 μm (H'-H'', I'-I'', J'-J'' and L). *n* = 3 brains (CRE1; B, B'), *n* = 6 (CRE2; C, C', H-H'',
798 K, M), *n* = 6 (CRE3; D, D'), *n* = 3 (CRE4; E, E', I-I'', K, M), *n* = 4 (CRE5; F, F'), *n* = 3
799 (CRE6; G, G', J-J', K, M).
800
801 **Figure 4. During regenerative neurogenesis, *mdka* CRE2, CRE4 and CRE6,**
802 **maintain radial glial EGFP expression, though show variability in the injured**
803 **brain hemisphere. A**, Schematic illustrating the experimental design and orientation
804 of telencephalic brain sections. Adult zebrafish were subjected to stab injury in the

right hemisphere of the telencephalon, and brains were collected and fixed at 5 days post-lesion (dpl). **B-G'**, EGFP expression from stable transgenic lines for CRE1 (B, B'), CRE2 (C, C'), CRE3 (D, D'), CRE4 (E, E'), CRE5 (F, F'), and CRE6 (G, G') is shown for both contralateral and ipsilateral sides (asterisks indicate ipsilateral/injured side) of the telencephalon. Rectangles in B-G indicate magnified regions shown in B'-G', respectively. Dashed lines mark the telencephalon contour (B)**. H,** Quantification of EGFP-positive and S100β-positive RGCs. The number of EGFP-positive RGCs in the injured (ipsilateral) hemispheres of CRE2, CRE4, and CRE6 transgenic lines is shown as a percentage relative to the corresponding contralateral side in boxplots. No significant differences were observed among CREs (*ANOVA*, $p > 0.05$). **I,** Stemness of EGFP-positive RGCs in CRE2, CRE4, and CRE6 was assessed. Relative proportions of type 1 (quiescent, $S100\beta^{+}/PCNA^{-}$) and type 2 (activated, $S100\beta^{+}/PCNA^{+}$) RGCs in contralateral and ipsilateral hemispheres are presented as stacked bar plots. **While no statistical differences were found among CREs in the contralateral hemisphere, a significant difference was observed between CRE2 and CRE6 in the ipsilateral (injured) hemisphere ($p < 0.01$). Representative confocal images used for quantifications in panels H and I are provided in Supplementary Figures S3C-D''' and S4B-D''', showing co-immunostaining for EGFP, S100β, and PCNA. Each data point represents an individual brain slice. Scale bars: 200 μm (B-G); 25 μm (B'-G'). Sample sizes: $n = 3$ brains (B, B'), $n = 4$ (C, C'), $n = 5$ (D, D'), $n = 3$ (E, E'), $n = 4$ (F, F'), $n = 3$ (G, G'), $n = 3$ for each CRE (H, I).

Figure 5. Combination of CREs enhances faithful transgene expression in both embryos and the adult telencephalon under homeostatic conditions. A, Schematic of the pTol2-mdkaCRE2346-gata2aPR:egfp-pA construct, in which a combination of CRE2, CRE3, CRE4, and CRE6 drives EGFP expression initiated by the *gata2a* promoter region (*gata2aPR*). **B-B''**, Comparison of EGFP transgene (B') and *mdka* mRNA (B'') expression in 24 hpf embryo. Merged EGFP and *mdka* mRNA signals (B) show co-localization primarily in the brain and spinal cord (white arrows). **C**, Merged EGFP and *mdka* mRNA expression in a transverse section of the adult telencephalon under homeostatic conditions. The magnified Dm region (dashed rectangle) is shown in D-D''. **D-D''**, Magnified views of the telencephalic Dm domain showing merged signals (D), EGFP driven by CRE2346 (green, D'), and endogenous *mdka* mRNA (magenta, D''). White arrowheads indicate RGCs in the ventricular zone

839 (VZ). **E,** Faithfulness of EGFP transgene expression driven by CRE2, CRE4, CRE6
840 and the combined CRE2346. EGFP expression in VZ of each CRE transgenic line was
841 compared with endogenous *mdka* mRNA. Data are shown as boxplots representing
842 the percentage of $EGFP^+$/$mdka^+$ double-positive cells relative to total $mdka^+$ cells.
843 Median values are indicated. Significant differences were observed between
844 CRE2346 and individual CREs (*ANOVA* followed by *Tukey's* test; CRE2346 vs CRE2
845 [$p < 0.01$], vs CRE4 [$p < 0.01$**], vs CRE6 [$p < 0.05$*]). The data for individual CREs
846 are identical to that shown in Figure 3K. **F-G**, Stemness analysis of RGCs labeled by
847 CRE2346-driven EGFP. EGFP-positive cells in the VZ of the telencephalic Dm domain
848 were categorized as type 1 (quiescent, $S100\beta^+$/$PCNA^-$) or type 2 (activated,
849 $S100\beta^+$/$PCNA^+$) using immunolabeling. **F-F'''**, Transverse telencephalon sections
850 showing EGFP (F'), PCNA (F''), S100β (F''') and merged image (F), highlighting type
851 1 and 2 RGCs under homeostatic conditions**. G,** Stemness of CRE2346-driven EGFP-
852 positive RGCs was assessed and compared to those of individual CREs in a stacked
853 bar chart. The individual CRE data are reused from Figure 3M. Mean ± standard
854 deviation of type 1 RGCs (as a proportion of EGFP-positive RGCs) is shown. Each
855 data point represents an individual brain slice. No significant differences were
856 observed among different CREs (*n.s.*; *Kruskal-Wallis* test, $p = 0.05$). Scale bars: 200
857 μm (B-B'' and C); 25 μm (D-D'', F-F'''). Sample sizes: $n = 3$ brains (C, D-D'', E); $n = 5$
858 brains (F-F''', G).
859
860 **Figure 6. Combination of CREs enhanced faithful transgene expression in the**
861 **adult telencephalon after brain injury. A-C''**, Merged images of EGFP expression
862 driven by CRE2346 (green) and endogenous *mdka* mRNA (magenta) in a transverse
863 section of the adult telencephalon during regenerative neurogenesis at 5 dpl. The
864 hemisphere ipsilateral to the injury is marked with an asterisk. **A**, Overview of the
865 telencephalon. Stippled rectangular regions indicate areas magnified in B-B'' (Dm
866 domain) and C-C'' (site of injury). **B-B''**, Magnified merged image of CRE2346-driven
867 EGFP (green, B') and endogenous *mdka* mRNA (magenta, B''). **C-C'**, Magnified
868 merged view at the site of injury (C), showing upregulated expression of CRE2346-
869 driven EGFP (green, C') and endogenous *mdka* mRNA (magenta, C''). **D,** The number
870 of S100β-positive RGCs expressing either CRE transgenes or endogenous *mdka*
871 mRNA in the hemisphere ipsilateral to the injury did not differ between CRE constructs

872 and the endogenous gene (*n.s.*; *Kruskal-Wallis* test, p = 0.11). The number of
873 ipsilateral RGCs is normalized to that of contralateral RGCs. **E**, In the CRE2346
874 transgenic line, EGFP levels in the ipsilateral hemisphere are significantly higher than
875 in the contralateral side (*Welch t*-test, $p < 0.001$***). Normalized integrated
876 fluorescence across brain slices is presented in arbitrary units (AU). **F-G**, Faithfulness
877 of (F) and ectopic (G) EGFP transgene expression driven by either CRE2, CRE4,
878 CRE6 or CRE2346 in contralateral ("c") and ipsilateral hemispheres ("I") after brain
879 injury. **F**, EGFP expression in VZ of each CRE transgenic line were compared with
880 endogenous *mdka* mRNA expression. Results are presented in boxplots showing the
881 percentage of cells double-positive for EGFP and endogenous *mdka* mRNA relative
882 to the total number of *Stemness*-positive cells. Significant differences were observed
883 between CRE2346 and each individual CREs (*Dunn's post hoc* test after *Kruskal–*
884 *Wallis*: CRE2346 vs CRE2 [$p < 0.01$**], vs CRE4 [$p < 0.01$**] and vs CRE6 [$p <$
885 0.001***]). No significant difference was observed between contralateral and
886 ipsilateral hemispheres in all cases (*n.s.*; *Dunn's post hoc* test after *Kruskal–Wallis*
887 analysis). **G**, Ectopic EGFP expression outside the VZ of each CRE transgenic line
888 are shown relative to the number of endogenous *mdka*-positive RGCs. Although no
889 significant difference was observed between contralateral and ipsilateral hemispheres,
890 CRE2346 showed significantly lower ectopic transgene expression compared to
891 CRE4 (Adjusted *p*-values in *Dunn* test following *Kruskal-Wallis* test; $p < 0.001$***) and
892 CRE6 ($p < 0.001$***). **H-J**, Evaluation of RGC stemness in the CRE2346 line using
893 PCNA and S100β immunostaining. **H-I'''**, Transverse section of the adult
894 telencephalon during regenerative neurogenesis at 5 dpl, showing the merged image
895 (H-I) of CRE2346-driven EGFP (green, H'-I'), PCNA (magenta, H''-I'') and S100β
896 (blue, H'''-I'''). The white rectangular regions in H-H''' are magnified in I-I''',
897 respectively. Representative type 1 ($S100\beta^+/PCNA^-$) and type 2 ($S100\beta^+/PCNA^+$)
898 RGCs are indicated (I-I'''). **J**, Stemness of CRE2346-driven EGFP-positive RGCs
899 compared to individual CRE lines and endogenous *mdka* mRNA ("*mdka*"). Pairwise
900 comparisons were performed using *Dunn*'s test following a significant *Kruskal–Wallis*
901 test (*n.s.* for p >= 0.05, * for $p < 0.05$, ** for $p < 0.01$ and *** for $p < 0.001$). The results
902 for hemispheres contralateral ("C") or ipsilateral ("I") to the injury are plotted adjacent
903 to each other. The data for CRE2, CRE4 and CRE6 are identical to Figure 4I. Each
904 data point represents an individual brain slice. Black solid dots indicate outliers. Scale
905 bars: 200 μm (A, H-H'''); 25 μm (B–B'', C-C'', I–I'''). Sample sizes: n = 4 brains (A, B-

906 B’’, C-C’’); *n* = 6 brains (CRE2346; D, H-H’’’, I-I’’’, J); *n* = 3 brains (E, F, G); *n* = 3 brains
907 (endogenous expression of *mdka*; D, J).

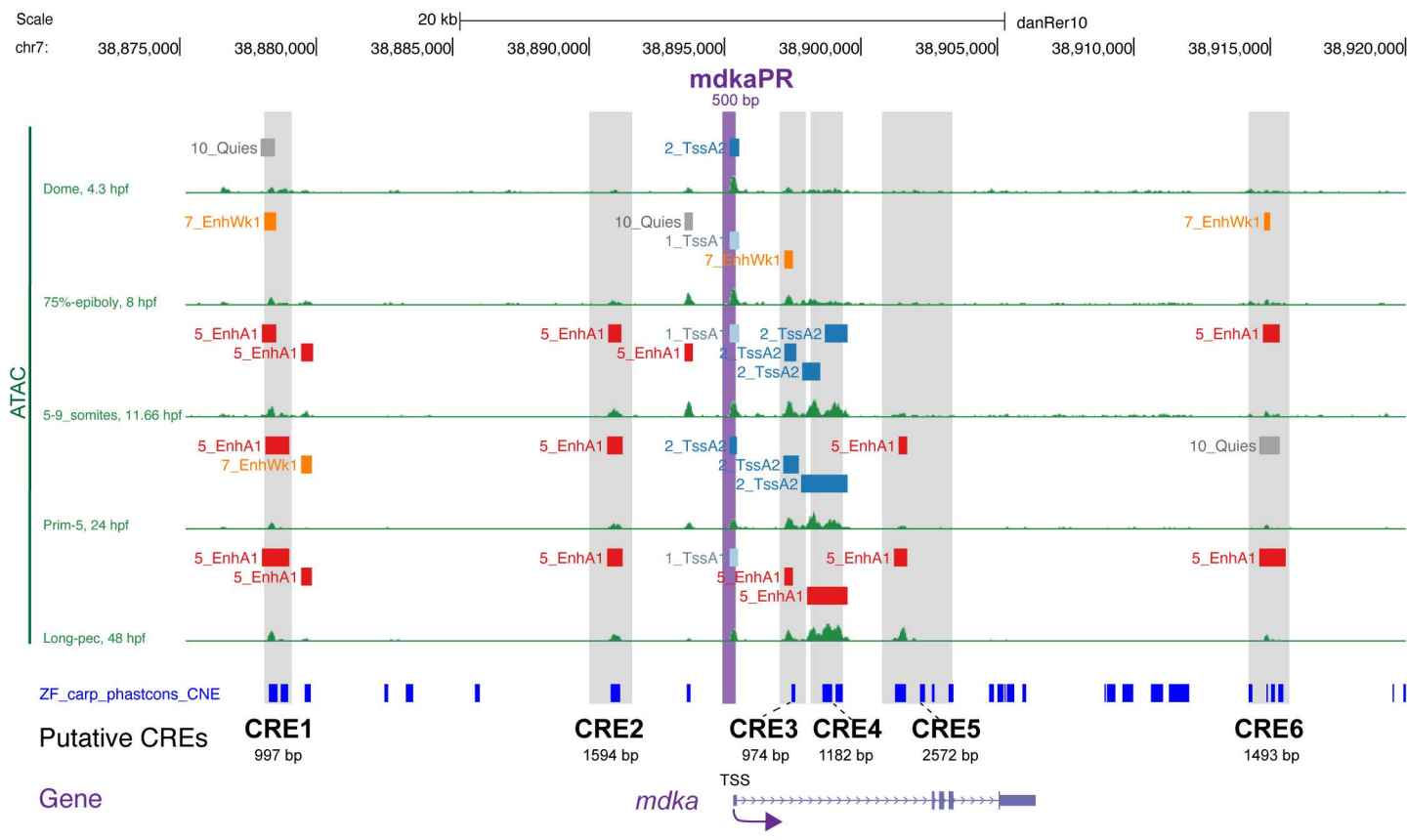
Scale
20 kb
danRer10
chr7:
38,875,000
38,880,000
38,885,000
38,890,000
38,895,000
38,900,000
38,905,000
38,910,000
38,915,000
38,920,000
mdkaPR
500 bp
ATAC
Dome, 4.3 hpf
75%-epiboly, 8 hpf
5-9_somites, 11.66 hpf
Prim-5, 24 hpf
Long-pec, 48 hpf
10_Quies
2_TssA2
7_EnhWk1
1_TssA1
5_EnhA1
ZF_carp_phastcons_CNE
Putative CREs
CRE1
997 bp
CRE2
1594 bp
CRE3
974 bp
CRE4
1182 bp
CRE5
2572 bp
CRE6
1493 bp
Gene
TSS
mdka

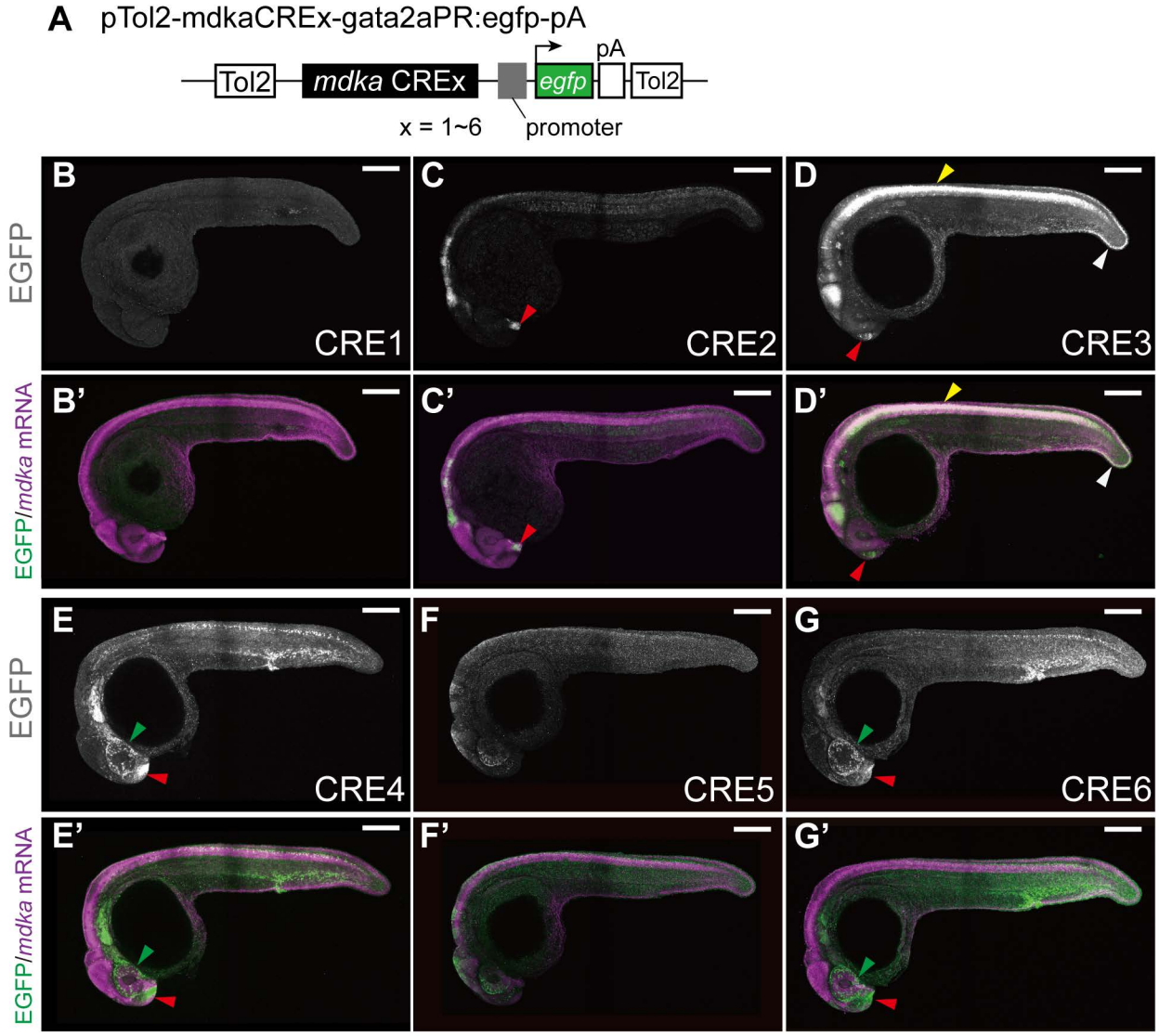
A
pTol2-mdkaCREx-gata2aPR:egfp-pA
Tol2
mdka CREx
egfp
pA
Tol2
x = 1~6
promoter
EGFP
EGFP/mdka mRNA
EGFP
EGFP/mdka mRNA
B
C
D
CRE1
CRE2
CRE3
B'
C'
D'
E
F
G
CRE4
CRE5
CRE6
E'
F'
G'

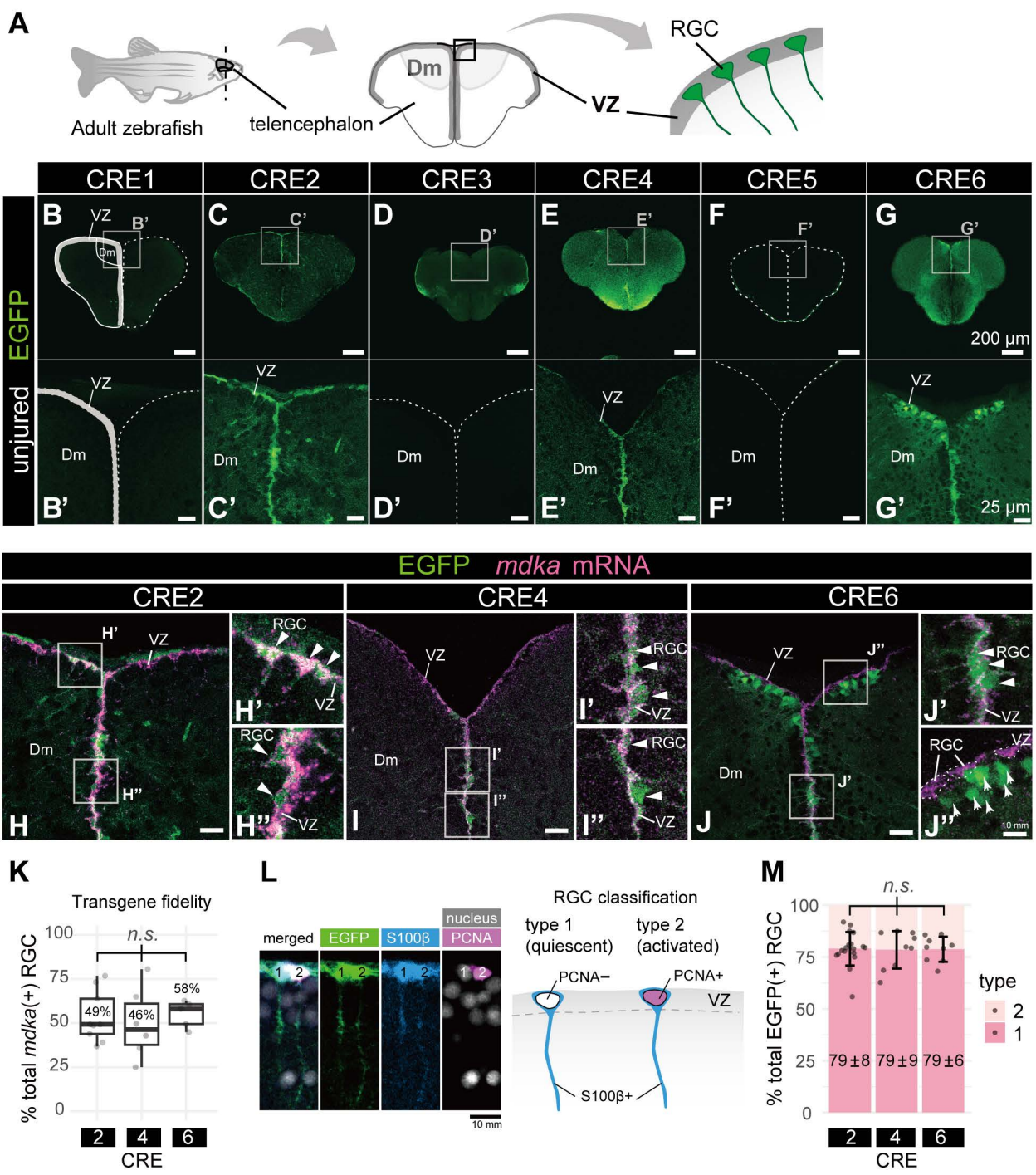
A
Adult zebrafish
telencephalon
Dm
VZ
RGC
CRE1
CRE2
CRE3
CRE4
CRE5
CRE6
EGFP
unjured
200 µm
25 µm
EGFP mdka mRNA
10 mm
K
Transgene fidelity
% total mdka(+) RGC
n.s.
49%
46%
58%
CRE
L
merged
EGFP
S100β
nucleus
PCNA
RGC classification
type 1 (quiescent)
type 2 (activated)
PCNA−
PCNA+
S100β+
M
% total EGFP(+) RGC
79 ±8
79 ±9
79 ±6
type

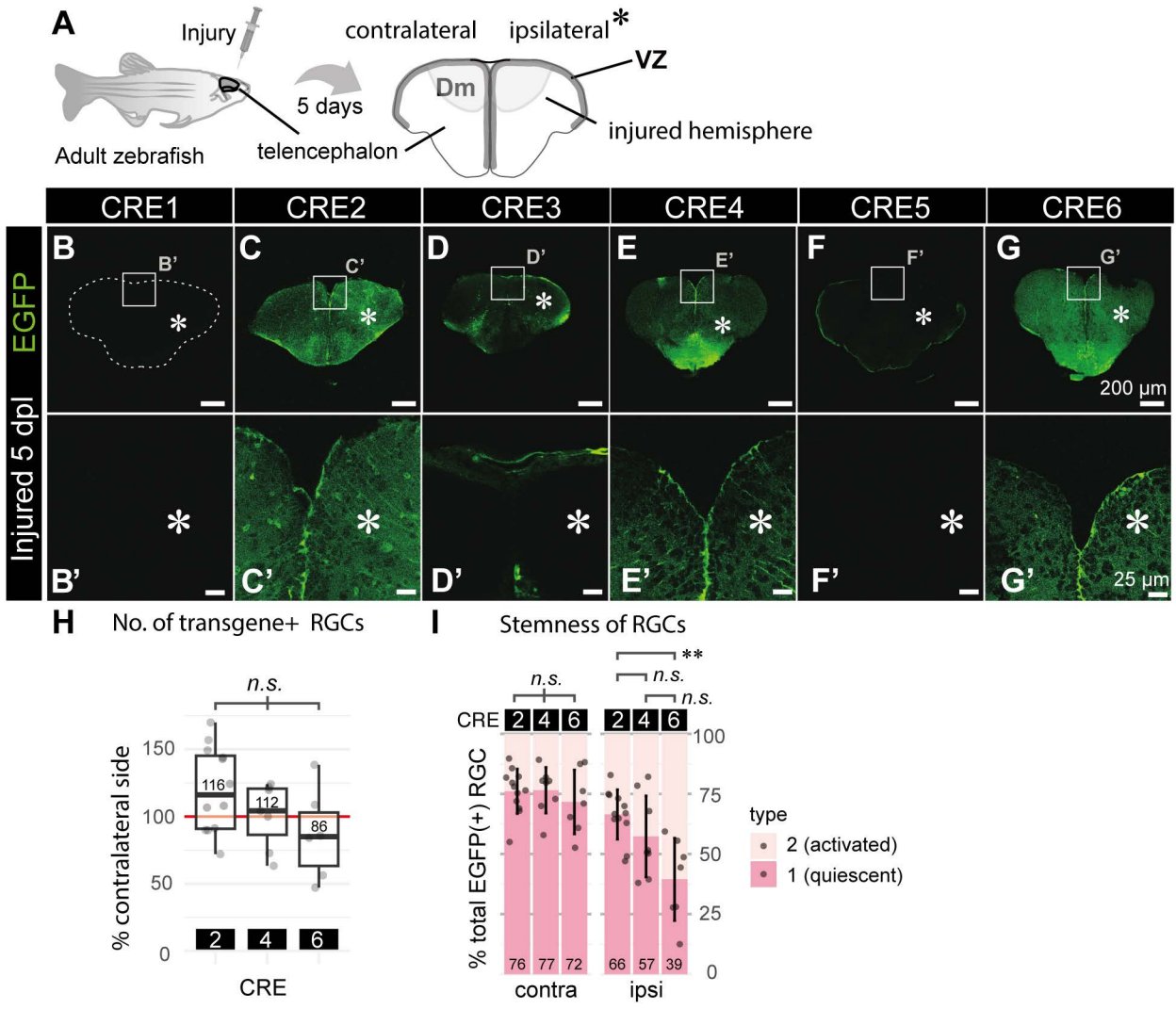
A
Injury
Adult zebrafish
5 days
telencephalon
contralateral
ipsilateral*
VZ
Dm
injured hemisphere
CRE1
CRE2
CRE3
CRE4
CRE5
CRE6
EGFP
Injured 5 dpl
B
B'
C
C'
D
D'
E
E'
F
F'
G
G'
200 µm
25 µm
H
No. of transgene+ RGCs
n.s.
% contralateral side
150
100
50
0
116
112
86
2
4
6
CRE
I
Stemness of RGCs
n.s.
**
n.s.
n.s.
CRE
% total EGFP(+) RGC
100
75
50
25
0
76
77
72
66
57
39
contra
ipsi
type
2 (activated)
1 (quiescent)

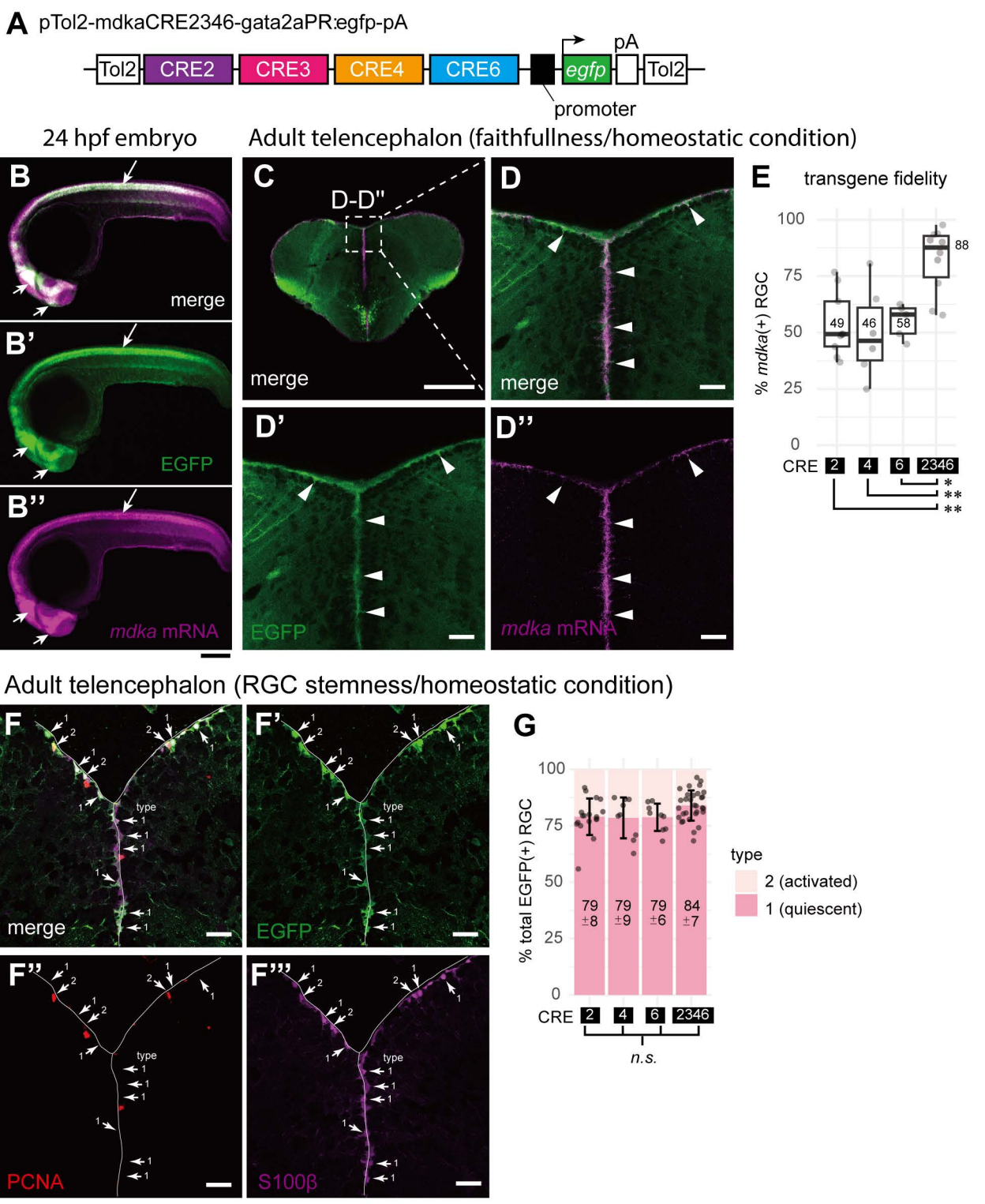
A
pTol2-mdkaCRE2346-gata2aPR:egfp-pA
Tol2
CRE2
CRE3
CRE4
CRE6
egfp
pA
Tol2
promoter
24 hpf embryo
Adult telencephalon (faithfullness/homeostatic condition)
B
merge
B'
EGFP
B''
mdka mRNA
C
D-D''
merge
D
merge
D'
EGFP
D''
mdka mRNA
E
transgene fidelity
% mdka(+) RGC
100
75
50
25
0
49
46
58
88
CRE
2
4
6
2346
*
**
**
Adult telencephalon (RGC stemness/homeostatic condition)
F
merge
F'
EGFP
F''
PCNA
F'''
S100β
type
G
% total EGFP(+) RGC
100
75
50
25
0
79 ±8
79 ±9
79 ±6
84 ±7
CRE
2
4
6
2346
n.s.
type
2 (activated)
1 (quiescent)

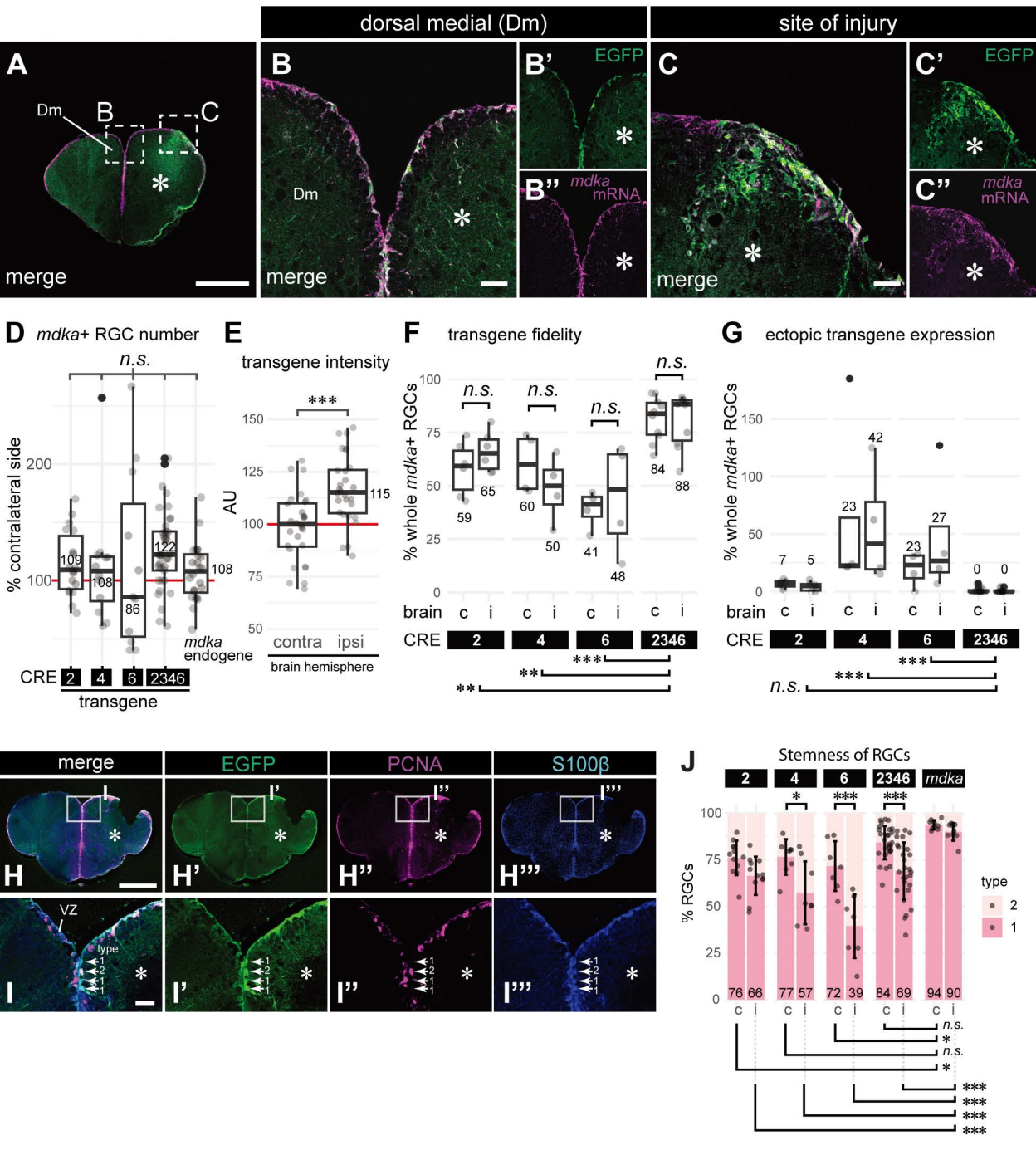
dorsal medial (Dm)
site of injury
A
Dm
B
C
merge
B
Dm
merge
B'
EGFP
B''
mdka mRNA
C
merge
C'
EGFP
C''
mdka mRNA
D
mdka+ RGC number
n.s.
% contralateral side
109
108
86
122
108
mdka endogene
CRE 2 4 6 2346
transgene
E
transgene intensity
***
AU
115
contra ipsi
brain hemisphere
F
transgene fidelity
% whole mdka+ RGCs
n.s.
59
65
60
50
41
48
84
88
brain c i c i c i c i
CRE 2 4 6 2346
***
**
**
G
ectopic transgene expression
% whole mdka+ RGCs
7
5
23
42
23
27
0
0
brain c i c i c i c i
CRE 2 4 6 2346
***
***
n.s.
merge
EGFP
PCNA
S100β
H
H'
H''
H'''
VZ
type
I
I'
I''
I'''
J
Stemness of RGCs
2 4 6 2346 mdka
% RGCs
type
2
1
76 66
77 57
72 39
84 69
94 90
c i c i c i c i c i
n.s.
*
n.s.
*
***
***
***
***